Automatic Interpretation of Small Strain Shear Modulus Measurement Using Bender Elements

Ionut Dragos Moldovan[1(✉)] and António Gomes Correia[2]

[1] CERIS, ICIST, Instituto Superior Técnico, Universidade de Lisboa, Lisbon, Portugal
dragos.moldovan@tecnico.ulisboa.pt

[2] Institute for Sustainability and Innovation in Structural Engineering (ISISE), School of Engineering, University of Minho, Guimarães, Portugal
agc@civil.uminho.pt
https://sites.google.com/site/ionutdmoldovan

Abstract. This paper reports on a novel procedure for the automatic calculation of small strain shear moduli in bender element experiments. The interpretation of the output signal in such experiments is notoriously difficult because the input wave gets distorted as it travels through the sample, hindering the visual comparison between the input and output signals. Conversely, the procedure described here maximises the correlation between the experimental output signal and its computational simulation and returns the shear modulus for which the maximum is attained. The maximisation procedure is encoded as a fixed point algorithm to remove its sensitivity to the initial choice of the shear modulus, and extend the convergence basin of the absolute maximum correlation over many local extrema.

Keywords: Bender element experiment · Small strain shear modulus · Model updating · Cross-correlation

1 Introduction

Piezoelectric bending devices (bender elements) are a cheap, versatile and reliable alternative to resonant column for measuring small-strain shear modulus of geomaterials (G_0). A ready-to-use bender element equipment costs far less than a resonant column apparatus, can be installed in both oedometers and triaxial devices, and yields measurements that are consistent with those of the resonant column [1,2].

A typical setup consists of two bender elements, situated at opposite ends of the sample of geomaterial. The controlled vibration of one of the bender elements (the emitter) induces a shear wave that propagates through the sample and whose arrival is read by the other bender element (the receiver) at the opposite end. The vibration of the receiver is translated into an electric signal (the output

A. G. Correia et al. (Eds.): ICITG 2019, SSGG, pp. 70–83, 2020.
https://doi.org/10.1007/978-3-030-32029-4_6

signal) which is delivered to the analyst. The arrival time of the shear wave must be identified in the output signal, enabling the computation of the propagation velocity, which is subsequently used to obtain the shear modulus.

The identification of the arrival time in the output signal is, however, notoriously difficult and uncertain, because the output signal is strongly affected by spurious reflections of the waves from the lateral boundaries of the sample [3], so its features differ substantially from the emitted (input) signal. This poses considerable challenges to the direct interpretation of the output signal, as most conventional approaches are based on the assumption that input and output signals are essentially similar [4].

In a recent couple of articles [5,6], we argued that a considerable amount of information useful to the interpretation of the output signal in bender element experiments can be acquired from their computational simulation. A numerical model capable of providing results that are consistent with those obtained in the laboratory opens the prospect of using model updating techniques for the recovery of G_0. Instead of trying to correlate signals that are different in nature (input and output signals), such techniques correlate the *output* signals obtained in the laboratory and using the numerical model. Since the correlation function features a high density of local extrema precisely in the region where the G_0 values of interest are located, conventional maximisation techniques would typically converge to a local rather than the global maximum. To avoid this, a fixed-point model updating technique was devised [6]. The method searches for the fixed point of the maximum cross-correlation between the experimental and simulated output signals. This fixed point is the predicted shear modulus. The method features an extremely wide attraction basin, meaning that it converges to the correct solution even for highly inaccurate initial predictions of G_0. Moreover, the convergence is exceptionally fast, rarely requiring more than three iterations to reach 1% accuracy.

A brief, practical introduction to the fixed-point method for the automatic interpretation of the output signal in bender element experiments is presented in this paper. For more details into the mathematical fundamentals of the method, the reader is advised to consult References [5,6].

2 Bender Element Tests and Their Interpretation

A typical bender element setup is illustrated in Fig. 1. The lateral vibration of the emitter creates three wave fronts: a shear wave front propagating in the direction normal to the vibration of the emitter and two compression wave fronts propagating laterally towards the lateral envelope of the container. The generation of the shear wave is the main objective of the experiment. Its propagation velocity enables the calculation of the shear modulus, which is typically done by using the continuum mechanics expression,

$$G_0 = \rho \cdot (v_S)^2 = \rho \cdot \left(\frac{h}{t}\right)^2 \tag{1}$$

where v_S is the shear wave velocity, ρ is the density of the material, t is the propagation time and h is the travelling distance of the wave, typically measured between the tips of the emitter and receiver bender elements.

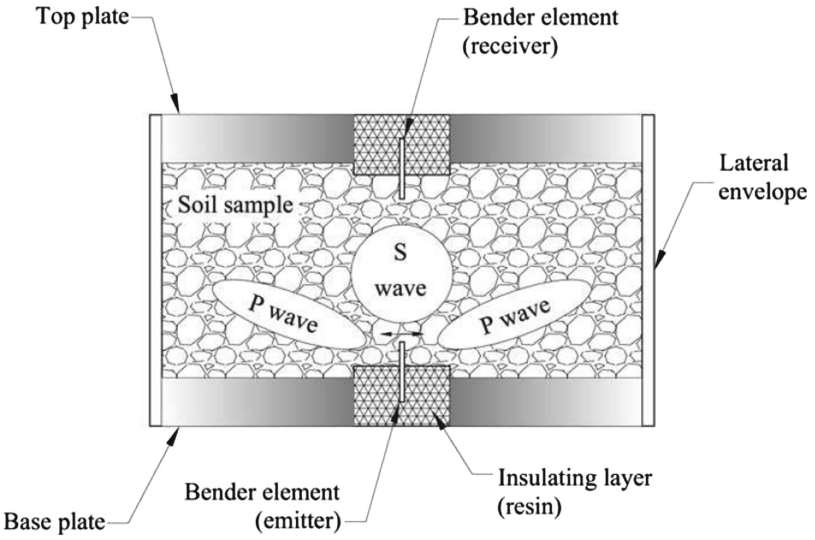

Fig. 1. Typical installation of bender elements.

In the ideal case, the shear wave reaches the receiver before the compression waves, and causes its mechanical deformation. The receiver converts this deformation into an electrical signal which is recorded by the data acquisition system. The travel time is measured based on the input and output signals, using either time domain or frequency domain approaches. Time domain approaches are used with pulse excitations and aim at reading the arrival time directly from the output signal. Frequency domain approaches are used with continuous input signals, whose frequency is continuously shifted. Since the wave pollution is common to both pulse and continuous signals, this presentation is focused on the former.

Assuming that a single sine pulse is applied to the sample, the ideal shape of the output signal recorded sufficiently far from the emitter is presented in Fig. 2. The interpretation of the output signal is not straightforward even for such ideal cases. Indeed, if the first arrival time is measured from $t = 0.0\,\mathrm{s}$, it is not clear which of the instants A, B or C should correspond to the arrival of the wave [7]. To avoid such difficulties, alternative strategies were suggested, namely: (i) to measure the travel time as the distance between the peaks of the input and output (point D) signals [8]; (ii) to use two successive output signals to measure the (double of the) same distance [3]; (iii) to use cross-correlation in order to quantify the global correspondence between the input and output signals as a function of time [9].

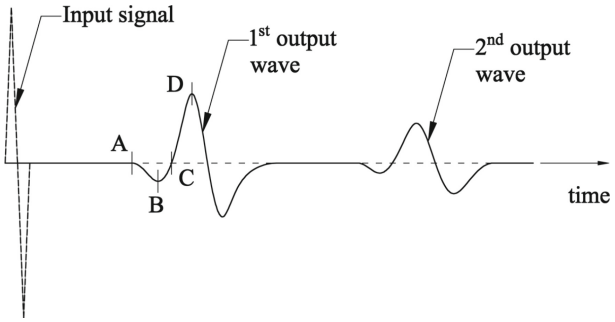

Fig. 2. Idealized shape of input and output signals.

The output signal recorded in the laboratory, however, is generally far from its idealization presented in Fig. 2. To illustrate this point, the output signal obtained on a dry Toyoura sand sample confined in an unpressurized rigid container and subjected to a pulse sine excitation of 2 kHz frequency is presented in Fig. 3. It is clear that ideal and real output signals bear little resemblance. Pinpointing the arrival time on the latter is even more difficult than on the former, for the following reasons:

- depending on the dimensions of the sample and the impedance of its lateral boundary, the fast, laterally propagating compression waves may arrive to the receiver before the shear wave;
- when the arrival of the actual shear wave occurs after the first compression wave front, its peak may be concealed by P wave interferences, as visible in the M-shaped pattern occurring between 2.4 ms and 2.6 ms in Fig. 3;
- upon reflection from the top platen, the intensity of the signal increases significantly, typically producing the oscillation with the highest amplitude.

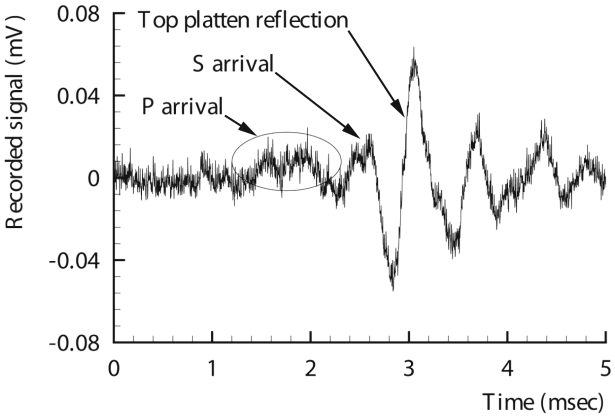

Fig. 3. Actual shape of an output signal.

The arrival of the shear wave may thus not correspond neither to the first nor to the strongest oscillation in the output signal.

Arguably the best practical demonstration of the huge difficulties faced by an analyst in interpreting the output signal in a bender element test was the parallel test conducted by the International Society of Soil Mechanics and Geotechnical Engineering (ISSMGE) in 23 laboratories of 11 countries, between 2003 and 2006. Identical samples of Toyoura sand were shipped to the participant laboratories, which were requested to measure their shear moduli and report back the results. While considerable discrepancies were found in all cases [10], these were particularly large for dry samples with low confining pressure, where the readings varied between roughly 4 and 140 MPa. This notoriously challenging situation is used in all applications presented in this paper.

3 Description of the Fixed-Point Interpretation Technique

3.1 Fundamentals

A common feature of the conventional methods for the interpretation of the output signal is that they are restricted to the direct use of laboratory data. Somewhat surprisingly, model updating techniques do not seem to have been applied to the interpretation of bender element experiments in a systematic manner. Model updating is a Reverse Engineering technique that aims at maximising the correlation between data measured experimentally and simulated using a numerical model. This maximisation is made by tuning some calibration parameter(s), which in our case is the small strain shear modulus. Therefore, instead of trying to match *experimental* input and output signals, model updating matches experimental and numerical *output* signals.

The mathematical optimisation problem that needs to be solved is defined as follows: *"Find the shear modulus G_0 that corresponds to the absolute maximum correlation between the output signals obtained experimentally and numerically".*

To solve the maximisation problem, we need to define mathematically the concept of correlation. Consider the discrete experimental and simulated output signals $E(t_i)$ and $S(G_0, t_i)$, where t_i, $i = \{1, 2, \ldots N\}$, are the N sampling instants. It is assumed that the sampling points t_i are the same for both signals.

The (instantaneous) correlation of the experimental and simulated output signals is a measure of their similarity. It is defined here as,

$$\mathcal{C}(G_0) = \sum_{i=1}^{N} \frac{E(t_i) \cdot S(G_0, t_i)}{\|E\| \cdot \|S\|} \tag{2}$$

where $\|E\|$ and $\|S\|$ are the L^2 norms of series E and S. Correlation (2) varies between zero, meaning no correlation at all, to ± 1, meaning full correlation. To compute the correlation, one needs to define the (tentative) shear modulus G_0

and the correlation window, that is, the values of t_1 and t_N. Some guidelines for the choice of the correlation window are given in Sect. 3.2.

The problem defined above can now be solved using any mainstream maximisation technique. However, our experience indicates that a large density of local maxima exist in the vicinity of the global maximum. For this reason, conventional maximisation techniques are bound to converge to a local maximum if the initial G_0 estimate is not very accurate, a requirement that may be as demanding and uncertain as the visual interpretation of the output signal itself. Moreover, since the numerical modelling of highly transient problems with high frequency contents requires very refined discretizations in both space and time, the evaluation of a high number of correlation points tends to be computationally expensive to the point of rendering this approach unfeasible.

The fixed-point method presented in the next section is devised to avoid such difficulties. It is based on the mathematical concept of cross-correlation. The cross-correlation of the experimental and simulated output signals is a measure of their similarity as a function of the time lag (τ) of the latter relative to the former. It is defined as,

$$\chi(G_0, \tau) = \sum_{i=1}^{N} \frac{E(t_i) \cdot S(G_0, t_i + \tau)}{\|E\| \cdot \|S\|} \tag{3}$$

Essentially, the cross-correlation compares the experimental signal $E(t_i)$ with shifted (lagged) versions of the simulated signal $S(G_0, t_i)$ and yields a measure of their similarity as a function of the time lag. The lag that maximises the cross-correlation is an excellent pointer for the choice of the shear modulus to be used in the next iteration of the maximisation process.

3.2 Fixed-Point Maximisation Procedure

The main steps of the fixed-point maximisation procedure are described next.

Step 1. *Analyse the experimental output signal and identify the time interval* $t \in [t_0, t_N]$ *where the cross-correlation between the experimental and simulated signals should be performed.*

It is probably natural for t_0 to correspond to the onset of the experiment, although the zone that is clearly silent in both the experimental and simulated signals may well be removed.

The choice of t_N is less obvious. It should be large enough to include the arrival time of the shear wave, but setting it too large may hinder the results if the model is not able to recover correctly the displacement field after the reflection of the shear wave from the receiver's end of the sample. For instance, the numerical model used for the numerical example in Sect. 4 does not consider the inertial vibration of the emitter after the voltage is switched off and does not explicitly include the receiver bender element into the model, so the part of the

output signal heavily affected by these features is not expected to be recovered correctly by the model. Since the main objective of the analysis is to pinpoint the *arrival* of the shear wave, the investment into the refining of the model such as to include all these effects is not justified, but the correlation window should not include the part of the signal which is not expected to be modelled accurately.

Step 2. *Analyze the experimental output signal and obtain a rough first estimate of the shear modulus* G_0.

The only obvious requirement for the choice of the initial G_0 estimate is that the arrival time calculated from expression (1) be well within the correlation window adopted in Step 1, to ensure that a substantial part of the simulated arrival signal stays within the window as well. It is therefore recommended that,

$$\frac{1}{(0.9 \cdot t_N)^2} \leq \frac{G_0}{(h^2 \rho)} \leq \frac{1}{(1.1 \cdot t_0)^2} \tag{4}$$

Step 3. *Construct the computational model, using the shear modulus estimate adopted in Step 2.*

Because of the physical complexity of the wave propagation phenomenon and the high frequency of the input pulse, it is not easy to construct a numerical model that yields local predictions consistent with those obtained experimentally. It is conjectured, however, that models able to capture the main features of the shear wave should be good enough for the application of the fixed point technique, since although the *value* of the maximum correlation is sensitive to the quality of the model, its *location* on the G_0 axis should be much less so.

Step 4. *Run the computational model and get the simulated output signal by computing the displacement time-history at the tip of the receiver bender element.*

Step 5. *Compute the cross-correlation* $\chi(G_0, \tau)$ *between the experimental and simulated output signals using definition (3), and identify the time lag* τ_{max} *that corresponds to its maximum:*

$$\tau_{max} = \underset{\tau \in [-t_N, t_N]}{\operatorname{argmax}} \ \chi(G_0, \tau) \tag{5}$$

Step 6. *Compute the shear modulus* $\mathcal{G}$ *that corresponds to the optimal time lag* τ_{max}*, according to expression,*

$$\mathcal{G} = \frac{h^2 \rho}{\left(h \sqrt{\frac{\rho}{G_0}} + \tau_{max}\right)^2} \tag{6}$$

and check if it stands within some acceptable tolerance from G_0.

This step corresponds to a convergence check, to be performed at the end of each iteration. If $\mathcal{G} \approx G_0$, the fixed point is found, the iterative process stops and the last G_0 estimate is output. If the difference between the value of the update function and the shear modulus estimate is large, the algorithm proceeds to the next step.

Step 7. *Update the tentative shear modulus as* $G_0 = \mathcal{G}$ *for the next iteration and go back to Step 2.*

A flowchart of the fixed point procedure is presented in Fig. 4.

4 Numerical Example

4.1 Experimental Setup

The fixed point technique presented in Sect. 3.2 is applied to the automatic evaluation of the small strain shear modulus of a sample of Toyoura sand. The tested material is identical to that used in the international parallel test conducted by the International Society of Soil Mechanics and Geotechnical Engineering [10]. Since the greatest difficulties in the interpretation of the results were reported for dry samples with low confining pressures, this situation is adopted here.

Specimens of the material described above are inserted in an acrylic mould (Fig. 5(a)). The mould has the height of 200 mm and internal diameter of 100 mm. Except for the reaction forces at the walls of the mould, no additional confinement pressure was applied to the sample. Two T-shaped bender elements, embedded in standard inserts (Fig. 5(b)), are attached at the opposite ends of the mould and inserted into the sample of Toyoura sand (Fig. 5(c)). Only the vertical bender element element is active in each insert. The bender elements are 11 mm in width, 1.8 mm in thickness and 7 mm in length, including the epoxy coating.

The experiments are performed using an harmonic pulse excitation with a frequency of 2.0 kHz. The output signal received by the bender element located at the top of the mould is presented in Fig. 6. Data cleansing is limited to the application of a low-pass filter to remove the high frequency noise caused by the recording apparatus. The signal is normalised to its maximum amplitude. The correlation window is identified on the output signal. It stretches from $t_1 = 0.0$ ms to $t_N = 3.0$ ms, roughly corresponding to the end of the first large amplitude of the output signal. The initial G_0 estimate is deliberately not chosen judiciously, to illustrate the convergence of the fixed point procedure when starting from an inaccurate G_0. Therefore, the arrival time estimate is simply picked as $t = 1.5$ ms, to which corresponds an initial shear modulus of $G_0^0 = 23.28$ MPa.

4.2 Numerical Model

The numerical model is constructed using hybrid-Trefftz finite elements [11]. The model is based on the well-known Biot's theory of porous media [12] and treats

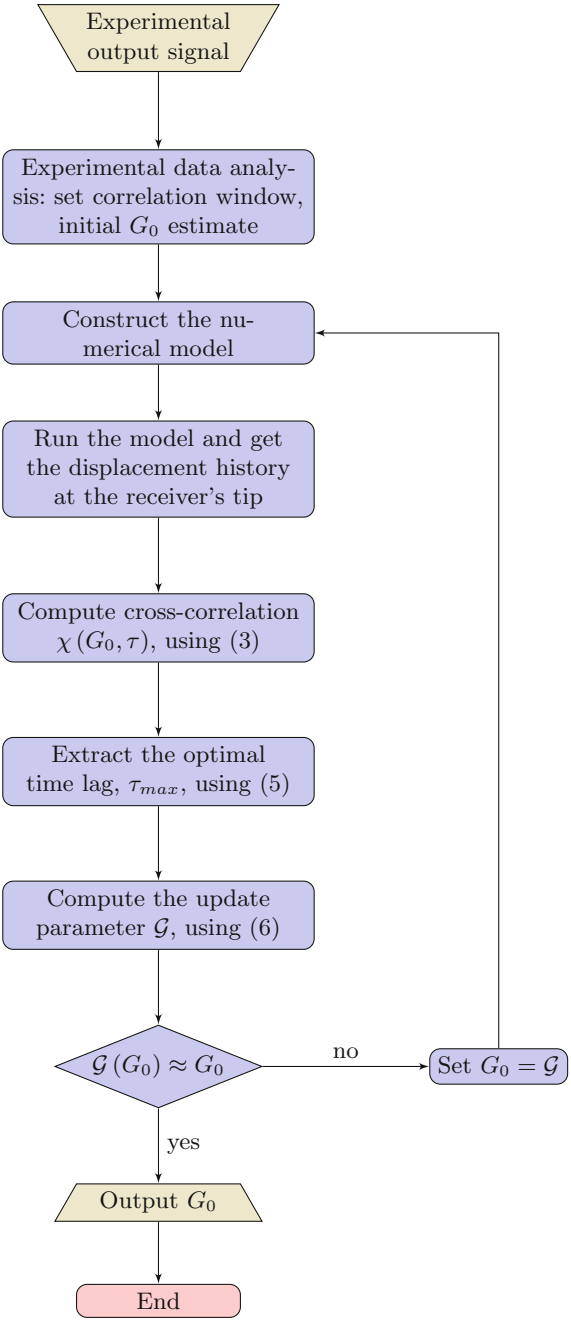

Fig. 4. Flowchart of the fixed point procedure.

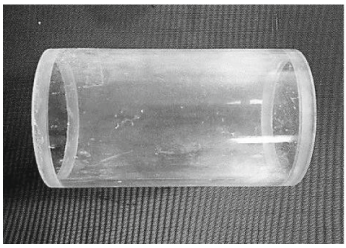

(a) Acrylic mould.

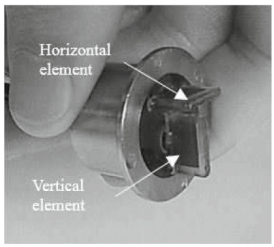

(b) T-shaped bender element and insert.

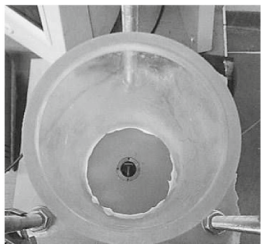

(c) Emitter embedded in the centre of the base platen.

Fig. 5. Bender element equipment.

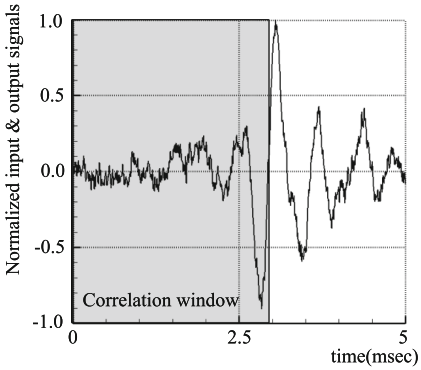

Fig. 6. Experimental output signal.

the material as a porous medium saturated with air. The full interaction between the solid and fluid phases is considered, including the influence of the seepage accelerations. Both phases are assumed compressible. Small deformations and linear-elastic material behaviour are assumed.

The numerical model uses a (very coarse) mesh of 66 hybrid-Trefftz finite elements to discretize the sample, as presented in Fig. 7.

Null normal displacement and fluid seepage are enforced on all exterior boundaries except for the sides corresponding to the emitter bender element and the upper horizontal side. A cantilever displacement with 1 μm amplitude and a sine pulse time variation is enforced on the emitter bender element (Fig. 7). All boundaries are considered frictionless, so the boundary tangential motion is free in both phases. On the upper horizontal sides, null tractions and pore pressures are enforced.

A single time step is used for the analysis of the wave propagation over an interval of 5.0 ms. The time basis is constructed using Daubechies wavelet and scale functions, with a resolution level of 5. The displacement time-history is

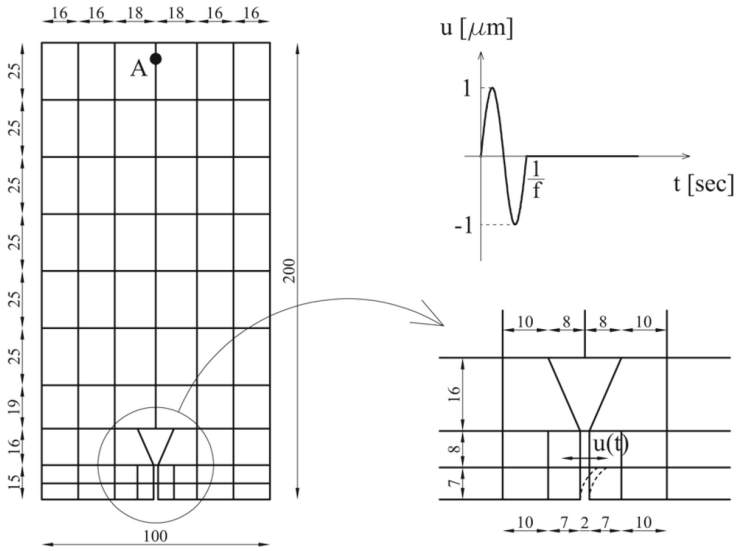

Fig. 7. Finite element mesh and input signal (dimensions are in mm).

recorded at point A (Fig. 7), corresponding to the tip of the receiver. However, the receiver is not explicitly included in the model.

4.3 Fixed Point Iterations

The fixed point model updating algorithm presented in Sect. 3.2 is applied to the automatic calculation of the shear modulus of the Toyoura sand, using the experimental output signals presented in Fig. 6. The initial shear modulus estimate, $G_0^0 = 23.28\,\text{MPa}$, corresponds to an arrival time $t = 1.50\,\text{ms}$. The procedure is considered to have converged when the absolute value of the shear modulus variation from one iteration to the next is below 1.0%.

The zero lag overlaying of the experimental and numerical output signals is calculated assuming $G_0^0 = 23.28\,\text{MPa}$ and presented in Fig. 8, along with a plot of the cross-correlation between the two signals.

The instantaneous correlation, $\mathcal{C}\left(G_0^0\right) = -0.411$, is indicated by a blue marker in the cross-correlation graph, while the best correlation point is highlighted with a red marker. In this case, the optimal time lag is $\tau_{max} = 0.308\,\text{ms}$. Substitution of the optimal lag into definition (6) yields the tentative shear modulus to be used in the next step, $G_0^1 = 16.03\,\text{MPa}$.

The process is now repeated using the new shear modulus, leading to the numerical output signal shown in Fig. 9(a). The instantaneous correlation between the experimental and numerical output signals is $\mathcal{C}\left(G_0^1\right) = 0.186$. The next optimal lag read from the cross-correlation plot is $\tau_{max} = 0.578\,\text{ms}$, and corresponds to an updated shear modulus $G_0^2 = 9.40\,\text{MPa}$.

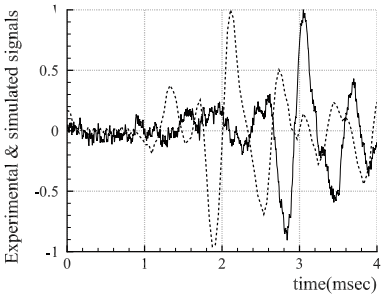

(a) Overlaying of experimental (solid line) and numerical (dashed line) output signals.

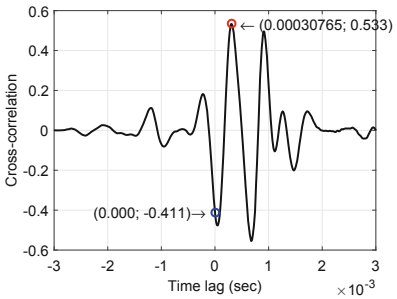

(b) Cross-correlation of experimental and numerical output signals.

Fig. 8. First iteration results.

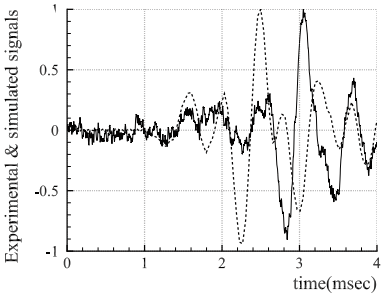

(a) Overlaying of experimental (solid line) and numerical (dashed line) output signals.

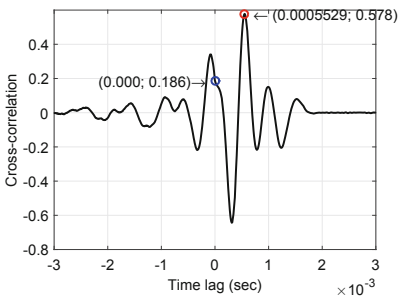

(b) Cross-correlation of experimental and numerical output signals.

Fig. 9. Second iteration results.

The third iteration is ran using this updated shear modulus and yields the numerical output signal and cross-correlation presented in Fig. 10. The instantaneous correlation is $\mathcal{C}\left(G_0^2\right) = 0.617$. Encouragingly, a single, large cross-correlation peak is identified in Fig. 10(b), at $\tau_{max} = -0.062\,\text{ms}$, corresponding to an updated shear modulus $G_0^3 = 9.91\,\text{MPa}$.

The fourth iteration is ran using this shear modulus and yields the numerical output signal and cross-correlation presented in Fig. 11.

According to the cross-correlation plot in Fig. 11(b), the zero lag cross-correlation is also the maximum correlation, at $\mathcal{C}\left(G_0^3\right) = 0.879$, meaning that the fixed point of the update function was found. The correlation between the experimental and simulated output signals is quite high, as confirmed by their overlaying in Fig. 11(a). The signals diverge after the reflection of the shear wave from the upper surface of the sample, since the receiver bender element and the residual vibration of the emitter bender element are not included into the model.

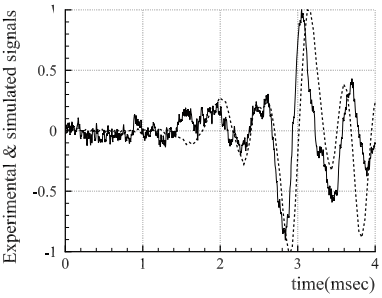

(a) Overlaying of experimental (solid line) and numerical (dashed line) output signals.

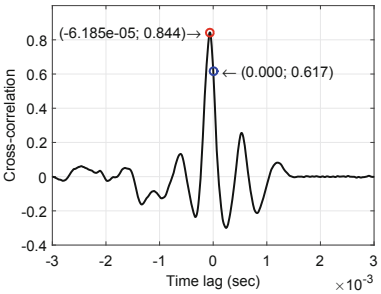

(b) Cross-correlation of experimental and numerical output signals.

Fig. 10. Third iteration results.

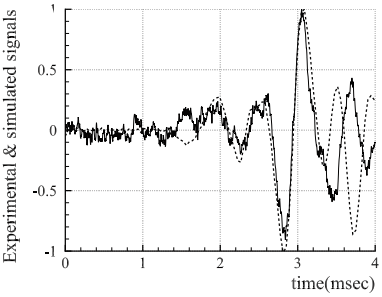

(a) Overlaying of experimental (solid line) and numerical (dashed line) output signals.

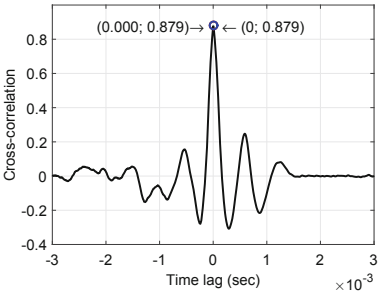

(b) Cross-correlation of experimental and numerical output signals.

Fig. 11. Fourth iteration results.

The iterative process is thus concluded, after four iterations. The final shear modulus predicted by the procedure is $G_0 = 9.91\,\text{MPa}$.

5 Conclusions

A new model updating procedure for the automatic computation of the small strain shear modulus in bender element experiments is presented in this paper. The technique is part of a coupled, experimental-numerical approach to the dynamic testing of geomaterials and is designed to avoid the uncertainty inherent to purely experimental methods.

The procedure aims at iteratively calibrating the shear modulus used in the numerical model to maximise the correlation between the experimental output signal and its computational simulation. However, the technique does not attempt to directly maximise the correlation, because the oscillatory nature of

the correlation function would render it too sensitive to the initial choice of G_0. Instead, the problem is encoded as a fixed point algorithm, where the tentative shear modulus of the next iteration is obtained from the cross-correlation of experimental and numerical output signals in the current iteration. This strategy removes the procedure's sensitivity to the initial choice of G_0, and extends the convergence basin of the absolute maximum correlation over many local extrema. The speed of convergence is also very large.

Funding Source. This research was supported by Fundação para a Ciência e a Tecnologia through project PTDC/EAM-GTC/29923/2017.

References

1. Dyvik, R., Madshus, C.: Lab measurements of G_{max} using bender element. In: Proceedings of the ASCE Convention on Advances in the Art of Testing Soils under Cyclic Conditions, pp. 186–196 (1985)
2. Santos, J., Santos, J., Ferreira, C., Pereira, C., Gomes Correia, A.: Assessment of shear modulus by different seismic wave-based techniques. In: Rinaldi, V.A., Zeballos, M.E., Clariá, J.J., (eds.) Deformation Characteristics of Geomaterials, pp. 374–381. IOS Press (2015)
3. Lee, J.-S., Santamarina, J.: Bender elements: performance and signal interpretation. J. Geotech. Geoenviron. **131**(9), 1063–1070 (2005)
4. Viana da Fonseca, A., Ferreira, C., Fahey, M.: A framework interpreting bender element tests, combining time-domain and frequency-domain methods. Geotech. Test. J. **32**(2), 1–17 (2009)
5. Moldovan, I.D., Gomes Correia, A., Pereira, C.: Bender-based G_0 measurements: a coupled numerical-experimental approach. Comput. Geotech. **73**, 24–36 (2016)
6. Moldovan, I.D., Gomes Correia, A.: Fixed point automatic interpretation of bender-based G_0 measurements. Comput. Geotech. **89**, 128–142 (2017)
7. Arulnathan, R., Boulanger, R.W., Riemer, M.F.: Analysis of bender element tests. Geotech. Test J. **21**(2), 120–131 (1998)
8. Viggiani, G., Atkinson, J.H.: Interpretation of bender element tests. Géotechnique **45**(1), 149–154 (1995)
9. Chan, C.-M.: Bender element test in soil specimens: identifying the shear wave arrival time. Electron. J. Geotech. Eng. **15**, 1263–1276 (2010)
10. Yamashita, S., Kawaguchi, T., Nakata, Y.M.T., Fujiwara, T., Shibuya, S.: International parallel test on the measurement of G_{max} using bender elements. Soils Found. **49**(4), 631–650 (2009)
11. Freitas, J.A.T., Moldovan, I.D., Cismaşiu, C.: Hybrid-Trefftz displacement element for bounded and unbounded poroelastic media. Comput. Mech. **48**, 659–673 (2011)
12. Biot, M.A.: Theory of propagation of elastic waves in a fluid saturated porous solid. II. Higher frequency range. J. Acoust. Soc. Am. **28**(2), 179–191 (1956)